

Photoluminescence Measurements and Molecular Dynamics Simulations of Water Adsorption on the Hydrophobic Surface of a Carbon Nanotube in Water Vapor

Yoshikazu Homma,^{1,*} Shohei Chiashi,^{2,†} Takahiro Yamamoto,^{3,‡} Kaname Kono,¹ Daiki Matsumoto,¹ Junpei Shitaba,¹ and Shintaroh Sato¹

¹*Department of Physics, Tokyo University of Science, Shinjuku, Tokyo 162-8601, Japan*

²*Department of Mechanical Engineering, The University of Tokyo, Bunkyo, Tokyo 113-8656, Japan*

³*Department of Liberal Arts, Faculty of Engineering and Department of Electrical Engineering, Graduate School of Engineering, Tokyo University of Science, Chiyoda, Tokyo 102-0073, Japan*

(Received 16 September 2012; published 9 April 2013)

Hydrophilicity or hydrophobicity is a macroscopic property of the surface, and its atomic scale understanding has not been established. We have studied adsorption of water molecules on the “hydrophobic” carbon nanotube surface at room temperature in water vapor. Based on optical measurements of individual single-walled carbon nanotubes suspended between micropillars in water vapor together with molecular dynamics simulations, we found that water molecules form a stable adsorption layer of 1–2 ML thickness on the nanotube surface and they show rapid adsorption and desorption transition at a critical pressure. This adsorption layer is created by lateral hydrogen bonding of water molecules confined in the weak van der Waals potential of the surface. In spite of hydrophobic hydration, carbon nanotubes exhibit hydrophobicity macroscopically.

DOI: [10.1103/PhysRevLett.110.157402](https://doi.org/10.1103/PhysRevLett.110.157402)

PACS numbers: 78.67.Ch, 68.43.-h, 92.40.Qk

Water can form a hydration layer on material surfaces. This is an indispensable property for living cells [1] and also influences the surface properties of materials in ambient air. Hydration clearly occurs on a hydrophilic surface immersed in water as a result of strong interaction between water molecules and the material surface. Recent atomic force microscopy studies revealed the ordered structure of water molecules on the surface [2–5]. A hydrophobic surface, on the other hand, has much weaker interaction with water molecules. Nevertheless, hydration takes place on the hydrophobic part of proteins in liquid water [6]. Then, a question arises: is a hydrophobic surface free from water molecules in the presence of water vapor? This is a crucial question in order to understand the nature of hydrophobicity in atomic scale.

Graphene is a simple model of hydrophobic surface to examine the interaction with water molecules because the van der Waals interaction originates only in a single atomic layer, and the surface is inert and flat owing to sp^2 carbon-carbon bonds. Here, we used single-walled carbon nanotubes (SWNTs) [7] to probe the behavior of water molecules on the graphene surface, since an SWNT is a rolled-up graphene and its hydrophobicity can be extended to that of graphene by taking into account the curvature effect. Because of the one-dimensional singular density of states of electrons, resonant optical measurements can be performed for an SWNT [8], and the effect of water molecule adsorption can be probed: the optical transitions in an SWNT are strongly influenced by the surrounding environment of the SWNT. Photoluminescence spectroscopy (PL) [9,10] can detect the condensation of molecules as a result of dielectric constant change [11,12]. Raman

scattering spectra [13] can indicate the kinetic interaction between adsorbed molecules and carbon atoms in the SWNT. Molecular dynamics (MD) simulation is also a powerful tool for exploring thermodynamic properties of water molecules around an SWNT as well as vibrational properties of a water-surrounded SWNT [14]. One thing we should note is that an SWNT also has an inner space. So, we selected as-grown SWNTs with closed ends.

We performed PL and Raman scattering spectroscopic measurements using individual SWNTs suspended between micropillars, while changing the temperature and water vapor pressure in an environmental cell. The growth and measurement conditions are the same as previous reports [15]. In short, SWNTs were directly grown on silica pillar structures (8 μm in height and positioned 7 μm apart) by ethanol chemical vapor deposition. For spectroscopy, a Ti:sapphire laser (690–850 nm) was used as the excitation laser. PL emission (900–1600 nm in wavelength) was measured with an InGaAs multiarray detector. The laser spot was 1–2 μm in diameter, and the laser power was lowered to 0.05 mW, avoiding additional heating by laser irradiation. The temperature of the sample (ranging from 20 to 45 $^\circ\text{C}$) was controlled by a Peltier temperature controller and the water vapor pressure (ranging from 1 to 2×10^3 Pa) in the environmental cell was controlled by a scroll pump and a mass flow controller.

Figure 1(a) shows a scanning electron microscopy (SEM) image of a suspended SWNT between a pair of silica pillars. Among the SWNTs grown on the pillar top area, only a few of them formed a singly isolated and suspended structure. Selecting perfectly isolated and high-quality semiconducting SWNTs was crucial for our

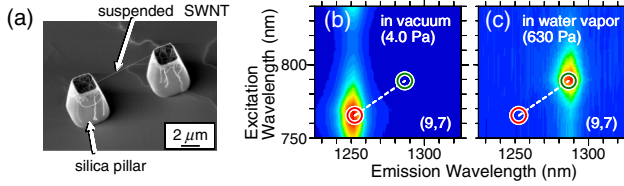


FIG. 1 (color online). PL from a singly suspended SWNT. (a) SEM image of SWNT suspended between silica pillars. PL maps measured from (b) a (9, 7) SWNT in vacuum (4.0 Pa) and (c) the same SWNT in water vapor (630 Pa) at room temperature (25 °C). The lower-left and center circles indicate the PL peak positions of the SWNT in vacuum and in water vapor, respectively.

investigation. Especially, we carefully selected suspended SWNTs which were not defective or chemically modified [15], and were closed at both ends. Since open-ended SWNTs showed an extra PL peak shift upon encapsulation of water [16], we could determine whether the SWNTs measured were closed or opened. PL maps, composed of PL emission spectra excited by varying the laser wavelength, were acquired from an individual SWNT in vacuum and in water vapor, and are shown in Figs. 1(b) and 1(c), respectively. The PL peak position shifted depending on the environment, i.e., vacuum or water vapor. The emission and excitation wavelengths in water vapor [Fig. 1(c)] were larger by 34 and 23 nm, respectively, than those in vacuum [Fig. 1(b)] [12] while the peak width was almost the same. The optical transition energies of the PL map in water vapor [the center circle in Fig. 1(c)] were almost equal to those of (9, 7) in ambient air [17].

The peak position shift occurred as a rapid transition when the water vapor pressure was varied, as shown in Fig. 2(a) for the emission spectra from a (10, 5) SWNT at various temperatures. The emission wavelength was independent of the water vapor pressure below the transition pressure P_t , and rapidly redshifted at P_t . This PL peak transition is similar to that observed in ethanol vapor [12], and is attributed to the adsorption and desorption of water molecules on the SWNT surface [11]. The surface adsorption of molecules increases the dielectric constant surrounding the SWNTs, and decreases the optical transition energy [18,19]. While SWNTs are not covered with adsorbed substances within vacuum, water molecules are adsorbed onto SWNTs at pressures above P_t . The discontinuous change of the density (coverage) at P_t from zero to almost saturation suggests that it is the first-order phase transition of water molecules on SWNT surface. Additionally, the adsorption and desorption phenomena are perfectly controlled by the temperature and pressure of the water vapor in the chamber, which indicates that the water layer is thermodynamically in equilibrium with the external water vapor phase.

The transition pressure P_t clearly depends on the SWNT temperature, as shown in Fig. 2(a). Based on the modified Langmuir model which involves the interaction between

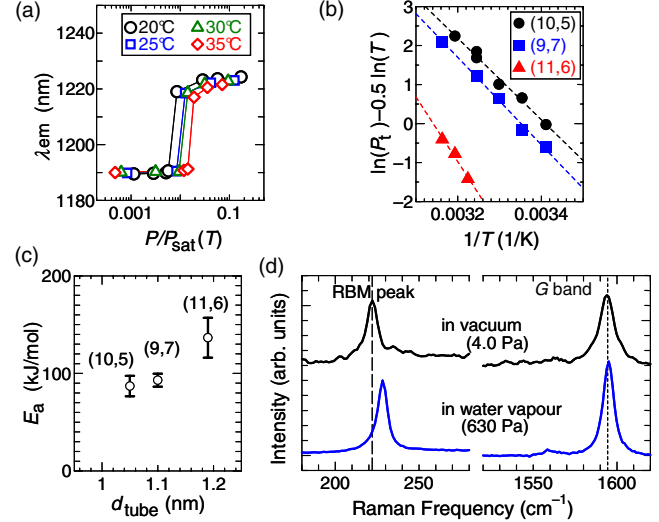


FIG. 2 (color online). Dependence of PL emission on the environment and chirality. (a) Water vapor pressure P and temperature T dependence of the emission peak wavelength λ_{em} for the (10, 5) SWNT. $P_{sat}(T)$ is the saturation vapor pressure. (b) Temperature dependence of the transition pressure $P_{sat}(T)$. Dashed lines were obtained using Eq. (1). (c) Tube diameter d_{tube} dependence of the activation energy E_a . (d) Raman scattering spectra (G band and RBM peak) from (10, 5) SWNT, measured in vacuum (4.0 Pa) and water vapor (630 Pa). The wavelength of the excitation laser is 785 nm.

adsorbates [20], the temperature dependence of P_t can be expressed as

$$P_t \propto \sqrt{T} \exp(-E_a/RT), \quad (1)$$

where T is the absolute temperature, E_a is the activation energy, and R is the gas constant [12]. The temperature dependence of P_t for three chiralities is shown in Fig. 2(b) and the present experimental data are well fitted to Eq. (1). The E_a value is shown in Fig. 2(c). In spite of the small temperature measurement range, the error of E_a is small, 7%–15%. The E_a values were around 100 kJ/mol, more than twice the heat of evaporation of bulk water, 44 kJ/mol at 25 °C [21]. The physical meaning of the large E_a is unclear at the moment and further theoretical studies are required to clarify it. Interestingly, E_a exhibited clear tube diameter dependence. The larger diameter SWNTs have lower P_t and the E_a increases with increasing tube diameter, as shown in Figs. 2(b) and 2(c). This diameter dependence means that the curvature of the tube surface hinders adsorption of water molecules, similar to the curvature effect expressed by Kelvin equation $p \propto \exp(-a/rT)$, where a is constant and r is curvature radius. This result predicts that water molecules more easily adsorb on the surface when the tube diameter becomes infinity, i.e., on the graphene surface. Note that the adsorption and desorption feature of water molecules for other carbon materials that have pores, slits, and defective structure as adsorption sites (amorphous carbon, active carbon [22], etc.) is much different from

those for SWNTs shown in Figs. 2(a) and 2(b). In the case of these carbon materials, their complex structures mainly contribute to water adsorption.

To examine the effect of water molecule adsorption, Raman spectra were measured simultaneously with PL measurement in vacuum and water vapor. For Raman scattering measurement, the excitation laser wavelength was set to 785.0 nm and the PL emission light and Raman scattering light were separated with two dichroic mirrors [23]. Raman spectra were obtained with a CCD array detector.

The result is shown in Fig. 2(d). While the G band around 1594 cm^{-1} did not show any change, indicating no charge transfer occurred between the water layer and the SWNT, the Raman frequency of the radial breathing mode (RBM) peak around 222 cm^{-1} clearly up-shifted above P_t in water vapor. Because RBM is a vibrational mode of the total symmetrical displacement of carbon atoms in the radial direction [13], the water adsorption directly affects the frequency of the vibration.

To analyze the molecular-scale structure of the water on the SWNT surface, we performed MD simulations of water molecules around the SWNT in the NVT ensemble using SCIGRESS ver. 2.3 (Fujitsu Ltd.). The temperature was controlled by the velocity scaling method. Periodic boundary conditions were imposed on all directions of the simulation cell consisting of a box with a volume $V = 5.5 \times 5.5 \times L\text{ nm}^3$, where $L = 8.52\text{ nm}$ is the length of an SWNT. A water molecule was expressed as the SPC/E force field [24]. The interaction between carbon atoms of an SWNT was expressed as an optimized Tersoff potential for graphene and SWNTs [25]. Universal force fields were used for the cross interaction between a water molecule and a carbon atom [26]. The velocity Verlet method was used to integrate the equation of motion with the time step of 0.5 fs. The time interval to calculate the thermal average of a physical quantity was taken to be several hundred ps after a system achieves equilibrium. The RBM spectrum of SWNTs can be extracted from the MD data in accordance with a similar way to Ref. [14].

Figure 3(a) shows an MD snapshot of 1000 water molecules around the (13, 0) SWNT at thermal equilibrium at 25°C . The diameter of (13, 0) SWNT is 1.05 nm, which is close to that of the measured (10, 5) SWNT (1.02 nm) shown in Fig. 2. The water molecules almost uniformly condensed on the SWNT outer surface, and clearly formed a layered structure, coexisting with the external vapor phase. The density distribution of water molecules along the radial direction from the central axis of the SWNT is presented for various numbers of water molecules ($N_{\text{H}_2\text{O}} = 600, 800, \text{ and } 1000$) in Fig. 3(b). Two peaks appear at $r = 0.84\text{ nm}$ and $r = 1.13\text{ nm}$, respectively, for any $N_{\text{H}_2\text{O}}$. As $N_{\text{H}_2\text{O}}$ increased, the density of water at $r = 0.84\text{ nm}$ approached a saturation value more quickly than that at $r = 1.13\text{ nm}$. For comparison, the density distribution of the bulk water around the (13, 0) SWNT ($N_{\text{H}_2\text{O}} = 1638$

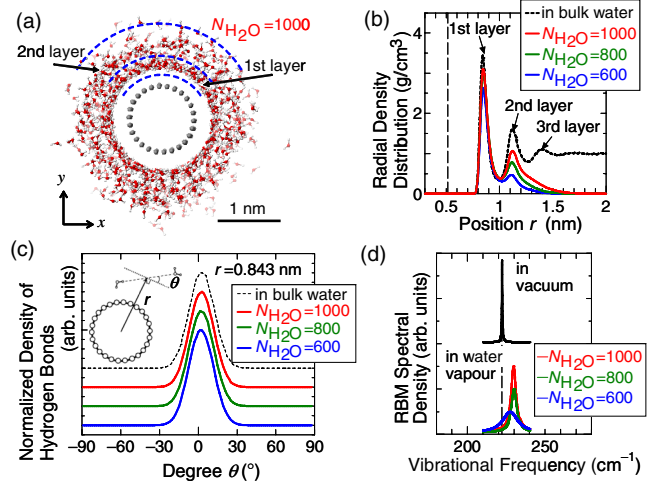


FIG. 3 (color online). MD simulation of (13, 0) SWNT and water molecules. (a) Snapshot of the SWNT and 1000 water molecules. (b) Radial distribution functions of water molecules around SWNT in a water vapor atmosphere (solid curves) and bulk water (dotted curves). The vertical dashed line at $r = 0.51\text{ nm}$ denotes the averaged radius of the (13, 0) SWNT. (c) Angle distribution between hydrogen bonds in the first layer and the tangential plane of the tube surface, which is normalized to the total number of hydrogen bonds in the first layer. (d) Calculated frequency of the RBM of (13, 0) SWNT in vacuum and water vapor.

in the cell with $V = 5.5 \times 5.5 \times 1.704\text{ nm}^3$) is plotted with the dotted curve in Fig. 3(b). The dotted curve has two clear peaks at $r = 0.84$ and 1.13 nm as well as a small third peak at $r = 1.40\text{ nm}$, and it reaches the density of the bulk water, 0.998 g/cm^3 , outside the third peak. This behavior is in excellent agreement with previous reports [14].

To clarify the detailed features of water molecules in each water layer, we investigated the orientation of hydrogen bonds between two water molecules in the layer. As depicted in the inset in Fig. 3(c), the orientation is expressed as the angle θ between a hydrogen bond and a plane perpendicular to the radial direction. Figure 3(c) shows the normalized density distribution of hydrogen bonds in the first layer as a function of θ . A peak appears at $\theta = 0$, which indicates that the water molecules in the first layer are connected with lateral hydrogen bonds. The position of the peak was maintained at $\theta = 0$ and the width of distribution did not change regardless of the number of water molecules $N_{\text{H}_2\text{O}}$. That is, the orientation of hydrogen bonds between the water molecules in the first layer is independent of $N_{\text{H}_2\text{O}}$ value and persists stably even when an SWNT is immersed in bulk water. In contrast to the first layer, the above-mentioned lateral hydrogen bonds could not be observed in the second layer and at more distant positions.

Figure 3(d) shows the simulated RBM of the (13, 0) SWNT in vacuum and wrapped with water molecules with various $N_{\text{H}_2\text{O}}$ values. The RBM frequency of the (13, 0) SWNT in vacuum was $f = 222\text{ cm}^{-1}$, and it up-shifted by

$\Delta f \approx +7 \text{ cm}^{-1}$ in the water vapor ($N_{\text{H}_2\text{O}} = 800$ and 1000). Interestingly, the up-shift of RBM frequency occurred once the water molecules began to condense on the SWNT, and then the up-shift showed little change after the first layer was formed. The up-shift of the RBM peak ($+7 \text{ cm}^{-1}$) in water vapor is in good agreement with the above experimental results shown in Fig. 2(d). The quantitative agreement of the adsorption effects on the vibrational properties ensures that the experimentally observed condensation of water molecules is essentially the same as the results of MD simulation.

Various theoretical papers have reported the confinement of water molecules in nanospace and some of them have pointed out the existence of structured water molecules in the vicinity of a hydrophobic surface [27]. Experimentally, two-layer crystalline ice films on graphene on Pt(111) were detected at low temperature and under ultrahigh vacuum conditions [28]. However, we should note that the surface of the graphene on Pt(111) is hydrophilic owing to the wetting transparency of graphene [29] and only suspended graphene exhibits its intrinsic hydrophobicity. In contrast, the water adsorption layer presented here appears purely on a graphene surface. The water layer on the hydrophobic graphene surface is thermodynamically in equilibrium with the external vapor and liquid phases around room temperature. The water layer can be present on other hydrophobic materials in general and it is regarded as “hydrophobic hydration” in water vapor.

In conclusion, we have complementarily performed experiments and theoretical simulations and shown that water molecules can form a structural layer of 1–2 ML thickness on the hydrophobic carbon nanotube surface as well as on the graphene surface as a result of hydrogen bonding network of water molecules. It exists at room temperature in the presence of water vapor and persists even in liquid water. The present results imply that nanotube and graphene exhibit hydrophobicity even though they are hydrated. The concept of hydrophobicity should be changed taking into account the interaction between water and hydrated surface as a solid-vapor interface.

This work was supported by MEXT KAKENHI Grant No. 19054015 and by JSPS KAKENHI Grant No. 24310094.

*Corresponding author.
homma@rs.tus.ac.jp

†Corresponding author.
chiashi@photon.t.u-tokyo.ac.jp

‡Corresponding author.
takahiro@rs.tus.ac.jp

- [1] G. Otting, E. Liepinsh, and K. W. Thrich, *Science* **254**, 974 (1991).
[2] T. Fukuma, M. J. Higgins, and S. P. Jarvis, *Biophys. J.* **92**, 3603 (2007).

- [3] K. Xu, P. Cao, and J. R. Heath, *Science* **329**, 1188 (2010).
[4] K. Kimura, S. Ido, N. Oyabu, K. Kobayashi, Y. Hirata, T. Imai, and H. Yamada, *J. Chem. Phys.* **132**, 194705 (2010).
[5] P. Cao, K. Xu, J. O. Varghese, and J. R. Heath, *Nano Lett.* **11**, 5581 (2011).
[6] Y. Cheng and P. J. Rossky, *Nature (London)* **392**, 696 (1998).
[7] S. Iijima and T. Ichihashi, *Nature (London)* **363**, 603 (1993).
[8] S. Reich, C. Thomsen, and J. Maultzsch, *Carbon Nanotubes, Basic Concepts and Physical Properties* (Wiley-VCH, Berlin, 2004).
[9] M. J. O’Connell, S. M. Bachilo, C. B. Huffman, V. C. Moore, M. S. Strano, E. H. Haroz, K. L. Rialon, P. J. Boul, W. H. Noon, C. K. J. P. Ma, R. H. Hauge, R. B. Weisman, and R. E. Smalley, *Science* **297**, 593 (2002).
[10] S. M. Bachilo, M. B. Strano, C. Kittrell, R. H. Hauge, R. E. Smalley, and R. B. Weisman, *Science* **298**, 2361 (2002).
[11] P. Finnie, Y. Homma, and J. Lefebvre, *Phys. Rev. Lett.* **94**, 247401 (2005).
[12] S. Chiashi, S. Watanabe, T. Hanashima, and Y. Homma, *Nano Lett.* **8**, 3097 (2008).
[13] A. M. Rao, E. R. S. Bandow, B. C. P. C. Eklund, K. A. Williams, S. Fang, K. R. Subbaswamy, M. Menon, A. Thess, R. E. Smalley, G. Dresselhaus, and M. S. Dresselhaus, *Science* **275**, 187 (1997).
[14] M. J. Longhurst and N. Quirke, *J. Chem. Phys.* **124**, 234708 (2006).
[15] K. Nagatsu, S. Chiashi, S. Konabe, and Y. Homma, *Phys. Rev. Lett.* **105**, 157403 (2010).
[16] S. Cambré and W. Wenseleers, *Angew. Chem., Int. Ed.* **50**, 2764 (2011).
[17] J. Lefebvre and P. Finnie, *Phys. Rev. Lett.* **98**, 167406 (2007).
[18] V. Perebeinos, J. Tersoff, and P. Avouris, *Phys. Rev. Lett.* **92**, 257402 (2004).
[19] Y. Ohno, S. Iwasaki, Y. Murakami, S. Kishimoto, S. Maruyama, and T. Mizutani, *Phys. Rev. B* **73**, 235427 (2006).
[20] A. W. Adamson, *Physical Chemistry of Surfaces* (John Wiley & Sons, New York, 1982), 4th ed.
[21] *CRC Handbook of Chemistry and Physics*, edited by D. R. Lide (CRC Press, Inc., Boca Raton, FL, 1994), 75th rev. ed.
[22] I. I. Salame and T. J. Bandosz, *Langmuir* **15**, 587 (1999).
[23] K. Kono, D. Matsumoto, S. Chiashi, and Y. Homma, *Surf. Interface Anal.* **44**, 686 (2012).
[24] H. J. C. Berendsen, J. R. Grigera, and T. P. Straatsma, *J. Phys. Chem. C* **91**, 6269 (1987).
[25] L. Lindsay and D. A. Broido, *Phys. Rev. B* **81**, 205441 (2010).
[26] A. K. Rappe, C. J. Casewit, K. S. Colwell, W. A. Goddard III, and W. M. Skiff, *J. Am. Chem. Soc.* **114**, 10024 (1992).
[27] S. Han, M. Y. Choi, P. Kumar, and H. E. Stanley, *Nat. Phys.* **6**, 685 (2010).
[28] G. A. Kimmel, J. Matthiesen, M. Baer, C. J. Mundy, N. G. Petrik, R. S. Smith, Z. Dohnalek, and B. D. Kay, *J. Am. Chem. Soc.* **131**, 12838 (2009).
[29] J. Rafiee, X. Mi, H. Gullapalli, A. V. Thomas, F. Yavari, Y. Shi, P. M. Ajayan, and N. A. Koratkar, *Nat. Mater.* **11**, 217 (2012).